Macromolecular Materials and Engineering
Open Access
www.mame-journal.de

# Toward a Green Chemistry Approach for the Functionalization of Melamine Foams with Silver Nanoparticles

*Ana Isabel Quilez-Molina,* Suset Barroso-Solares, Miguel Ángel Rodríguez-Pérez, and Javier Pinto**

**The growing popularity of silver nanoparticles in the field of nanotechnology has created the necessity of developing new sustainable synthesis methods. This study presents a new green in situ functionalization method of melamine foams with silver nanoparticles. The synthesis pathway and the influence of the processing parameters are optimized to phase out 100% of polluting and dangerous solvents while maximizing silver transfer. A deep study of the morphological and chemical changes of the synthesized silver nanoparticles successfully demonstrated that water can be used as the only solvent for obtaining active melamine foams with potential application in multiple fields. Results showed that rising reaction temperatures from environmental to mild conditions (40 °C and 60 °C) is crucial for obtaining high functionalization yields with this green method. Following the optimum fabrication conditions using only water, highly functionalized melamine foams showed a great amount of ultrafine silver nanoparticles distributed over the porous structure.**

## 1. Introduction

Among the commercial products that encompass nanomaterials, silver nanoparticles (AgNPs) are the most well-developed metal nanoparticles.[1] Their excellent physicochemical characteristics, high stability, biocompatibility, and lower cost with respect to other noble metals have brought them to the forefront of nanotechnology research.[2,3] These features have fostered the generation of new commercial products with widespread applications in diverse sectors, including food industry, energy, catalysis, medicine, sensors, etc.[2–4] For example, silver nanoparticles present unique optical properties that have allowed the fabrication of sensitive and naked-eye visible colorimetric sensors of a wide range of molecules.[5–7] Besides, its excellent antibacterial activity against a wide spectrum of microorganisms has been used to prevent microbial proliferation in the food packaging industry,[8] water cleaning,[9,10] and wound healing devices.[11]

The usual method to obtain the reduced form of silver nanoparticles (AgNPs), also called zero-valent, is based on the reduction of cationic ions ($Ag^+$) through the use of reducing agents. Nevertheless, the use of free-silver nanoparticles has been extensively limited because they present a strong tendency to agglomerate, which diminishes their activity and modifies their properties.[12,13] Moreover, there is a great concern over the damage caused by the leaching of the nanoparticles into the environment.[4,14,15] Immobilizing nanoparticles into a substrate has been presented as a promising method to guarantee the safety and sustainability of the material.[14,16] Moreover, a strong anchoring of the nanoparticles can avoid the formation of aggregates leading to a large polydispersity that reduces the efficiency of their activity.[4,17]

Polymers have been presented as excellent substrates for metallic nanoparticles that provides a wide range of applications (e.g., catalysis, sensor, drug delivery, etc.).[15,18,19] The functionalization method selected is strongly correlated to the final size, shape, size distribution, and morphology of the silver nanoparticles, which define the final properties of the material.[20] The incorporation of nanoparticles is usually performed using two techniques defined as ex situ, which means that the nanoparticles are synthesized first, and then added to the premade polymer, or in situ, when silver is synthesized directly within the polymer matrix by reduction of Ag salts ($Ag^+$).[20,21] Generally, the in situ method is preferred because the polymer

A. I. Quilez-Molina, S. Barroso-Solares, M. Á. Rodríguez-Pérez, J. Pinto
Cellular Materials Laboratory (CellMat), Condensed Matter Physics, Crystallography, and Mineralogy Department, Faculty of Science
University of Valladolid
Campus Miguel Delibes, Paseo de Belén n° 7, Valladolid 47011, Spain
E-mail: anaisabel.quilez@uva.es; javier.pinto@uva.es

A. I. Quilez-Molina, S. Barroso-Solares, M. Á. Rodríguez-Pérez, J. Pinto
BioEcoUVA Research Institute on Bioeconomy
Calle Dr. Mergelina, Valladolid 47011, Spain

S. Barroso-Solares, J. Pinto
Archaeological and Historical Materials (AHMAT) Research Group, Condensed Matter Physics, Crystallography, and Mineralogy Department, Faculty of Science
University of Valladolid
Campus Miguel Delibes, Paseo de Belén n° 7, Valladolid 47011, Spain

The ORCID identification number(s) for the author(s) of this article can be found under https://doi.org/10.1002/mame.202300178



**DOI: 10.1002/mame.202300178**

interaction avoids the agglomeration of nanoparticles obtaining higher performance.[21] However, embedding nanoparticles into the polymeric matrix could reduce their interaction with the environment, crucial for some applications like catalysis and water remediation.[12,22,23] This drawback could be partially overcome by using polymeric porous scaffolds, which could provide a higher active surface incrementing the nanoparticle activity.[12,24]

Melamine foam (MeF) is a commercially available polymer foam with an open porous structure and high porosity.[25,26] The great success of MeF can be explained because of its three-dimensional (3D) framework structure, which confers excellent absorption, mechanical, and insulation properties, lightweight, etc.[25,27] These properties have attracted the attention of researchers to use MeF as scaffolds for containing active nanoparticles, and for obtaining functional materials with a large spectrum of applications as catalysts,[28] water remediation devices,[26,29] and thermal insulators,[30] among others.[31,32] Regarding the development of water remediation devices, MeFs have been successfully functionalized with hydrophobic compounds, like reduced graphene oxide,[33,34] to obtain excellent oil-water separation devices, as well as with metal-organic frameworks (MOF), for the removal of a wide variety of water pollutants (e.g., dyes,[29] and mycotoxins[32]).

However, most of the fabrication routes involve multiple, time-consuming, and complex steps that require the use of diverse reagents to overcome the high tendency of nanoparticles to form aggregates and the poor adhesion between the nanoparticles and the polymer matrix.[21,35] For instance, the method proposed by Deng et al.,[10] to fabricate melamine foams decorated with silver nanoparticles and graphene consisted of a first preparation of the graphene oxide, which include the use of aggressive reagents (e.g., sulfuric acid and potassium permanganate), followed by the reduction and fixation of the silver salt and modified graphene oxide into the melamine foam.

On the contrary, Pinto et al.[24] developed a one-step method to obtain antibacterial MeF using only the neat substrate and a silver precursor ($Ag^+$) solution. In this work, the melamine skeleton acted as a reducing agent of the silver precursor generating zerovalent silver nanoparticles well-anchored to the polymer surface. Moreover, the content of silver nanoparticles in melamine foam reached up to 18 wt.%, outperforming most of the multiple-step methods found in the literature.[11,36] However, this method still has a harmful effect on the environment through the use of a hazardous solvent, tetrahydrofuran (THF) in high concentrations. Many studies collect the adverse consequences of THF to the environment and human health, such as carcinogenic effects, nervous system dysfunction, and DNA damage.[37–40]

Herein, the full substitution of THF by water was addressed through the optimization of the operating conditions of the nanoparticles synthesis (solvent ratio, reaction time, staticity, and temperature). A detailed study of the physicochemical properties of the functionalized melamine foams and silver nanoparticles anchored was performed using multiple characterization techniques (e.g., infrared spectroscopy, SEM, TEM, and XPS). This study results in the obtention of well-dispersed and ultrafine (<12 nm) AgNPs stably anchored to the melamine foam using water as the only solvent. For this to happen, the employment of moderate reaction temperatures was fundamental to obtain considerable amounts of silver functionalized in aqueous media. In the end, a nontoxic, clean, cost-effective, and sustainable one-step procedure was developed to obtain highly functionalized silver-melamine foams without compromising the advantageous tridimensional porous structure.

## 2. Results and Discussion

### 2.1. Microstructural Analysis

**Figure 1** displays the cross-section images of the dry functionalized foams after shaking in the precursor solution for 1, 3, and 7 days, as performed in our previous article.[24] All micrographs exhibited the characteristic open porous structure of melamine foams. The highly 3D porous structure guaranteed the rapid uptake and transport of the precursor solution into the foam. A detailed visual inspection indicated that the melamine structure remained unspoiled after the fabrication treatment in all samples. The SEM micrographs of MeF exposed to the different solvent ratios ($H_2O$:THF) for 7 days (Figure S1 of Supporting information) confirmed the innocuous effect of the solvent on the polymer structure. This indicated that the final functional materials obtained will benefit from the high porosity and surface area of the pristine MeF. In addition, the SEM micrographs exhibited bright nanoscale structures dispersed over the foam surface. A deeper analysis performed with the STEM-EDS revealed that the bright clusters corresponded to the silver nanoparticles, confirming the successful grafting of the AgNPs on the MeF surface, Figure S2, Supporting Information. The ability of the melamine foam to carry out the in situ anchoring of AgNPs was already reported in our previous work.[24] The SEM images reported in Figure 1 suggest that the density and distribution of the silver nanoparticles changed with the presence of THF and the exposure time, observing a greater presence of agglomerates with the water ratio and time of the processing.[24,41] Additional SEM images of the melamine foams using a different synthetic method: static, shaking, and stirring, after a certain reaction time of 7 days was reported in Figure S3, Supporting Information.

### 2.2. Study of the Mechanism Reaction Through FTIR Spectroscopy

The chemical characterization of the silver-functionalized melamine foams was performed using infrared spectroscopy. As schematically represented in **Figure 2**a, the silver synthesis is based on the redox reaction between the positively charged silver ion ($Ag^+$) and the amine group ($-NH_2$) located in the melamine foam skeleton. Herein, the $-NH_2$ group will reduce the positively charged silver salt ($AgNO_3$) molecules to $Ag^0$ and oxidize to oxime (=N—OH).[24] This synthesis mechanism of silver nanoparticles on melamine foams was demonstrated in our previous work.[24] The comparative study of the infrared spectra of the neat melamine foam and the melamine foam after soaking in the reaction solution can prove the success of the reaction. Figure 2b displays the infrared spectra of pristine MeF and two representative samples of MeF doped with silver nanoparticles (AgMeF_B_20_5_5d, and AgMeF_B_20_20_5d). The spectra of the rest of the samples containing AgNPs (AgMeF) are reported in Figure S4a (see Supporting Information).

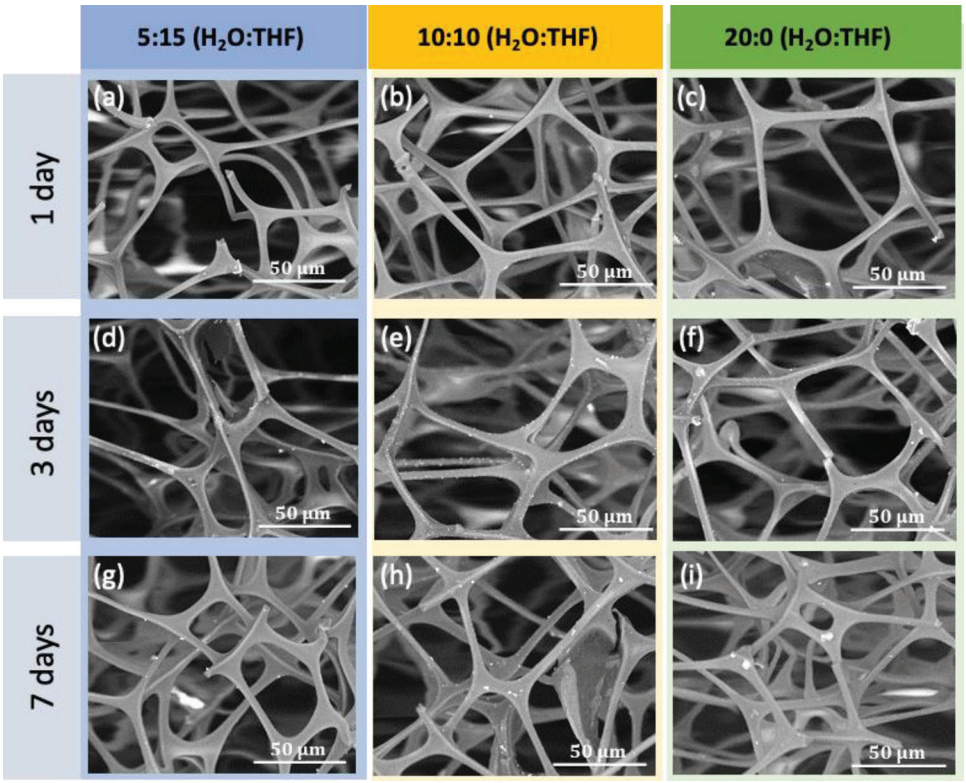


**Figure 1.** SEM images of the cross-section of MeF samples processed via shaking with a solvent ratio ($H_2O$:THF) of 5:15 v:v after a) 1 day, b) 3 days, and c) 7 days of soaking. MeF samples treated with a solvent ratio ($H_2O$:THF) of 10:10 v:v for d) 1 day, e) 3 days, and f) 7 days of soaking. Samples processed with a solvent ratio ($H_2O$:THF) of 20:0 v:v, for g) 1 day, h) 3 days, and i) 7 days of soaking.

In Figure 2b, MeF has an intense width peak located at 3335 $cm^{-1}$ that corresponded to the stretching vibration of the secondary amine (—$NH_2$) and imino (—NH—) groups. At 2950 $cm^{-1}$ and 2980 $cm^{-1}$ appeared the symmetric and asymmetric bands were attributed to the $\nu(CH_2)$, while the bands at 1540 $cm^{-1}$ and 1330 $cm^{-1}$ were assigned to the stretching vibration modes of (C═N) and (C—N) of the triazine ring, respectively. Bands at 1480 $cm^{-1}$ and 1160 $cm^{-1}$ referred to the bending vibration modes of methylene (—$CH_2$), while the stretching band of hydroxymethyl groups (—$CH_2$—OH) was located at 1010 $cm^{-1}$. Finally, the bending vibration of the triazine ring was located at 810 $cm^{-1}$.[28,42–44]

Regarding the functionalized AgMeF samples, the infrared spectra did not show peaks related to the presence of Ag-NPs because silver has no active vibration modes in infrared spectroscopy.[35] The most noticeable change was identified in the peak at 1300 $cm^{-1}$, where the vibration band of the O—H in-plane bending of the oxime (═N—OH) group can be observed. The deconvolution of this peak is shown in Figure 2c and resulted in two peaks corresponding to the stretching vibration of the C—N bond of the melamine foam, $\nu$(C—N) (1330 $cm^{-1}$) and the O—H in-plane bending of oxime, $\delta$(O—H) (1285 $cm^{-1}$), marked in yellow and red respectively. The area of the vibration peak $\delta$(O—H) of different melamine samples was used to quantify this functional group, which can be related to the reaction yield, by using the same infrared peaks of untreated MeF as reference. The samples under evaluation were kept under shaking for 1 or 7 days in different $H_2O$: THF solvent ratio solutions (5:15, 10:10, and 20:0 v/v) and subtracted by the neat melamine foam processed under the same solvent ratio conditions. The resulting areas are reported in Figure 2d. As observed, there is a positive correlation between the reaction time and the presence of THF. Samples soaked in the precursor solution for 1 day showed values of the area very similar to neat foams, indicating the low functionalization yield independent of the solvent ratio. The favorable effect of the THF in the foam functionalization was clearly noticed after 7 days.

### 2.3. Quantification of Silver in Melamine Foams

The quantification of the metal nanoparticles was performed by considering the residue resulting from the thermal decomposition of MeFs and functionalized AgMeFs foams as reported elsewhere.[41] **Figure 3** displays the percentage of silver (wt.%) included in melamine foams after stirring, shaking, and staying static for 3, 5, and 7 days in the precursor solution with different $H_2O$:THF solvent ratios. The silver content in foams ranged from 0.7 wt.% to 5.2 wt.%, with better results in samples soaking under stirring for longer times (7 days) and in the presence of THF. These conclusions are in concordance with those reported previously in the infrared section. Samples treated for 1 day were excluded because the low concentrations of silver (<1 wt.%) may be under the detection limit of the instrument.

 

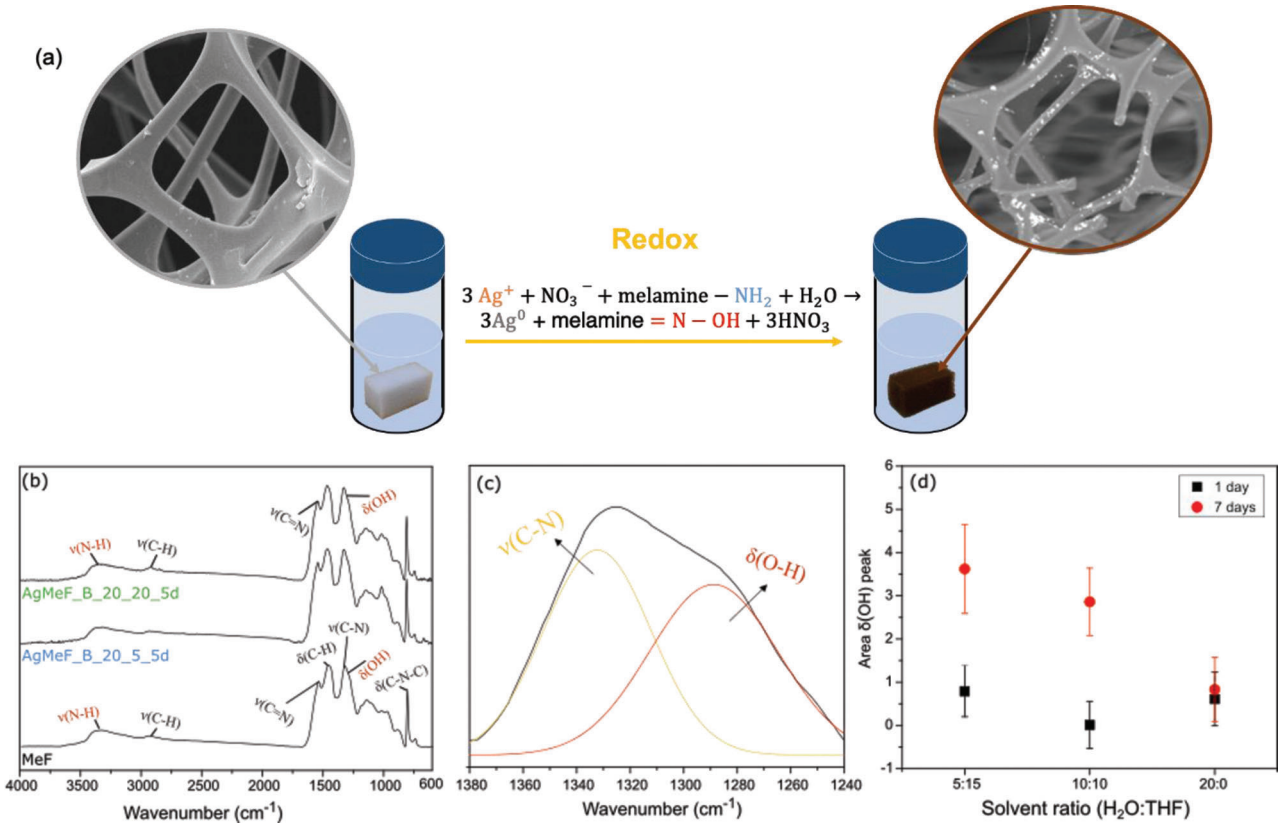


**Figure 2.** a) Scheme of the redox reaction between silver cations and amine located in the melamine skeleton. b) The infrared spectra and peaks assignation of the neat melamine foam (MeF), AgMeF_B_20_20_5d, and AgMeF_B_20_20_5d. c) The deconvolution of the peaks associated with the O—H in-plane bending of oxime, $\delta$(O-H), in red, and (C—N) group of the triazine ring, in yellow. d) The area of the peak belonging to the O—H in-plane bending of oxime ($\delta$(O—H)) was calculated for samples with a different solvent ratio and different soaking days (1 day and 7 days).

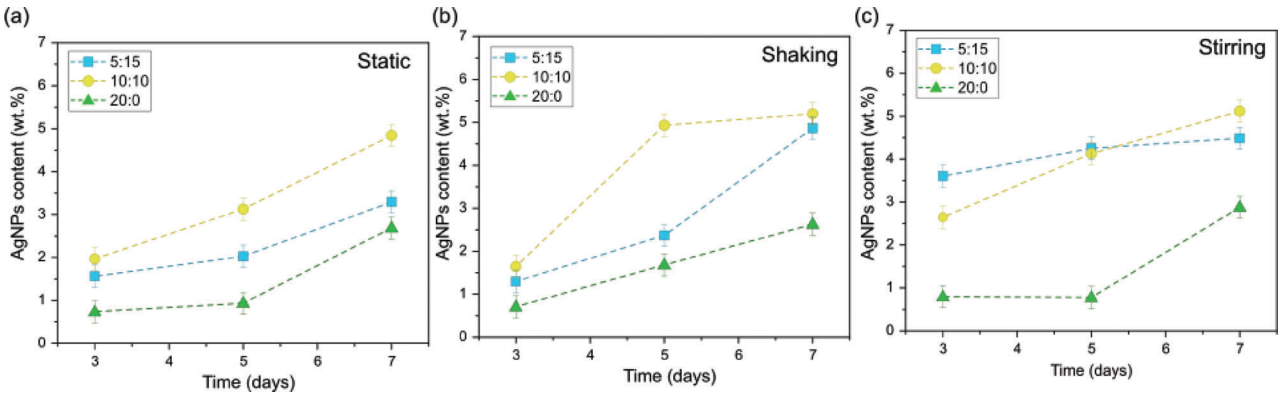


**Figure 3.** Content in silver nanoparticles of melamine foams fabricated in a) static, b) shaking, and c) stirring conditions.

The outstanding capability of THF of upgrading the activity of the metal catalyst has been already reported in different processes, like in lignocellulose fractionation,[45] among others.[46–48] Herein, the positive effect could be associated with the chemical nature of the solvents used, water is protic, and THF is an aprotic solvent.[45,47,48] In the fabrication of materials with catalytic activity via solvent impregnation of metal nanoparticles in porous substrates, protic solvents (water) have proven to interact through hydrogen bonds with the substrate, reducing the interaction between the matrix and the metallic salt.[47,48] THF, as an aprotic solvent, is unable to form hydrogen bonds with the matrix obtaining higher dispersion of nanoparticles and better performance.[47,48]

The content of silver using water showed a maximum value of 2.9% with a stirring time of 7 days. This green synthesis method gave functionalization yields comparable with other porous substrates found in bibliography.[11,49] For example, Karumuri et al.[14] fabricated antibacterial carbon foams with similar silver

 

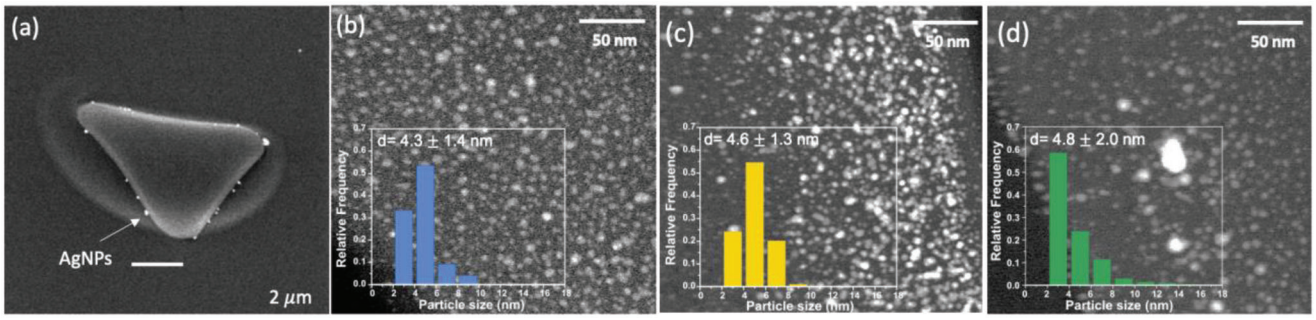


**Figure 4.** a) Cross-section STEM-HAADF micrograph of the foam edge of AgMeF_20_C_5_7d, selected as a representative sample. STEM-HAADF micrographs of b) AgMeF_C_20_5_7d, c) AgMeF_C_20_10_7d, and d) AgMeF_C_20_20_7d samples. The corresponding particle size histograms are shown in the insets.

concentrations ranging from 1.5 to 2.5 wt.% through a two-step method using dimethyl sulfoxide and Tri sodium citrate as reducing and stabilizing agents. The content of silver nanoparticles was only overcome by chitosan foams and melamine foams with concentrations ranging from 2 to 24 wt.%, and 0.2 to 18.6 wt.%, respectively.[18,24] However, high contents of nanoparticles do not ensure optimal performance regarding the material activity, as they can lead to agglomerates. In fact, in our previous study, it was demonstrated that, even when silver contents up to 18.6 wt.% were available in melamine foams, samples containing only 1.8 wt.% of silver showed excellent antibacterial properties, and no further improvement was provided by higher silver contents.[24] This occurs because the material activity is strongly influenced by the size distribution and morphology of the anchored nanoparticles.[18]

### 2.4. Characterization of Silver Nanoparticles

A deep analysis of the characteristics of the silver nanoparticles anchored in samples fabricated under the best processing conditions (i.e., stirring after seven days) was performed using TEM images. The silver nanoparticles are clearly distinguished in the cross-section STEM-HAADS micrographs of the foam edge as bright clusters reported in **Figure 4**a. The lack of nanoparticles inside the sample revealed that the functionalization reaction occurred only on the surface of the foam. The STEM-HAADF micrographs of AgMeF_C_20_5_7d, AgMeF_C_20_10_7d, and AgMeF_C_20_20_7d samples and particle size distribution histograms (inset) are displayed in Figure 4b–d. These images confirmed the proper dispersion of nanoparticles overall in the polymeric framework for all cases. The histograms of the particle size distribution display an average size of 4.3 ± 1.4 nm, 4.6 ± 1.3 nm, and 4.8 ± 2.0 nm for AgMeF_C_20_5_7d, AgMeF_C_20_10_7d, and AgMeF_C_20_20_7d, respectively. Interestingly, the particle sizes obtained are far below than those observed in other polymeric composites fabricated with similar processing methods.[50–52] For example, the size of silver nanoparticles anchored to polyacrylonitrile nanofibers reported by Phan et al.,[50] was determined ≈12–14 nm, which corresponds to three times the average size of the silver-functionalized melamine foams obtained in this work. This result is of noticeable relevance because, as it is well known, the performance of silver-functionalized materials is strongly associated with a low particle size.[16,51]

In Figure S5a,b, the HRTEM images of the AgNPs revealed that silver nanoparticles mainly exhibited sphere-like morphology and that they accumulate in some cases forming aggregates. The mean size of the silver aggregates was calculated by analyzing the bright clusters evidenced by the SEM images at high magnifications. The average diameter of the silver aggregates ranged from 220 nm to 341 nm, for AgMeF_C_20_10_7d and AgMeF_C_20_20_7d, respectively. This indicates that, in addition of increasing the particle size, using only water as a solvent also promoted the formation of silver aggregates. The presence of aggregates, if significant, can negatively affect the performance of the properties of the silver nanoparticles by reducing the active surface.[12,13] The percentage of silver in aggregates with respect to the total content of silver gradually increased with the water: THF ratio, from 6.07% in AgMeF_C_20_5_7d to 19.85% in AgMeF_C_20_20_7d. Moreover, the surface density of the silver nanoparticles for the functionalized samples showed values ranging from $2.0 \times 10^{10}$ to $1.3 \times 10^{10}$ Ag NPs $mm^{-2}$, while AgMeF_C_20_10_7d, which showed the greater value of surface density of silver aggregates, presented $1.9 \times 10^{4}$ aggregates $mm^{-2}$. The notable differences in the order of magnitude between the free Ag NPs and agglomerates, ≈6–7 orders of magnitude, highlighted the good dispersion and coating of the nanoparticles in these materials, as well as the minor occurrence of aggregates. All these values are represented in Table S2 of Supporting Information.

### 2.5. Effect of Temperature on the Functionalization of Foams

This section will search for the enhancement of the functionalization degree in water by performing the reaction at moderate temperatures. In the literature it is found that the temperature has a strong influence on the kinetic of the silver nanoparticles synthesis reactions, resulting in a change in the growth and aggregation mechanisms of the silver nanoparticles.[53,54] The photographs of the foams fabricated using only water as solvent under different temperature conditions (40 and 60 °C) are displayed in **Figure 5**a. From first sight, the temperature seemed to affect noticeably the foams functionalization due to the appreciable color change, from light brown to a greater darker brown

 

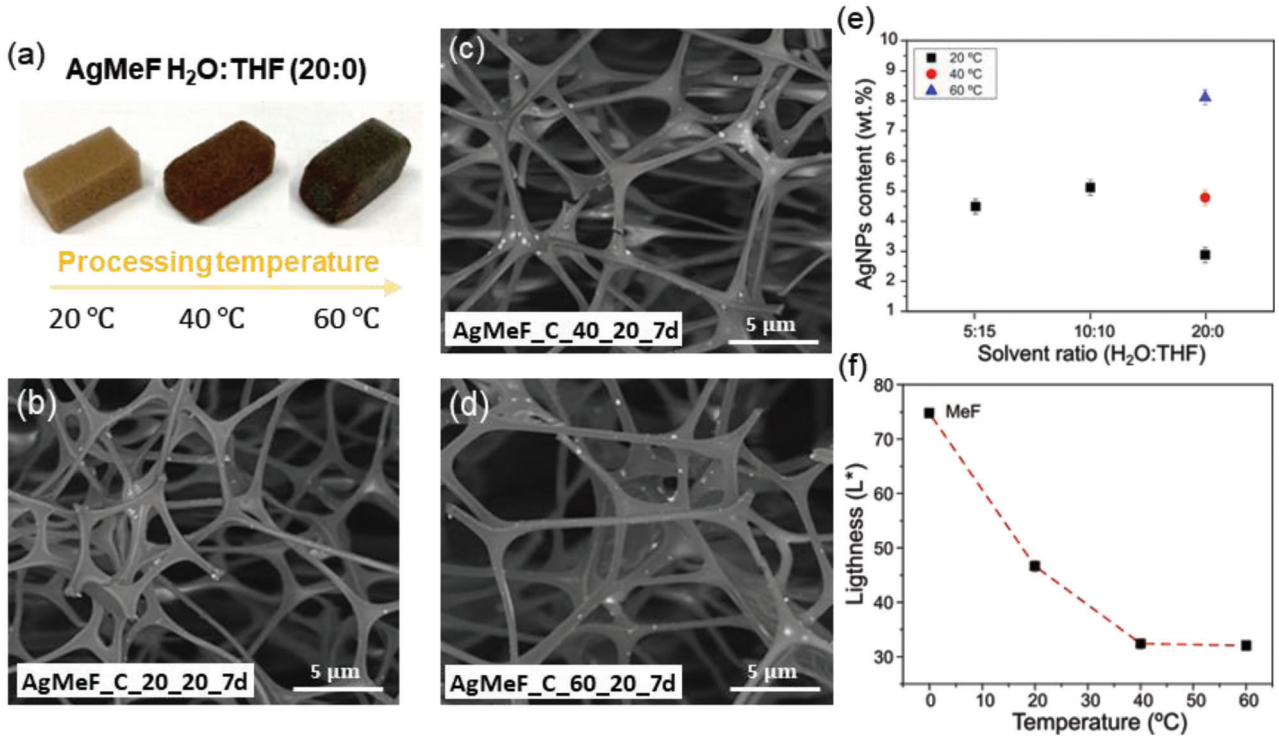


**Figure 5.** a) Photographs of the AgMeF functionalized with a $H_2O$:THF (20:0) at different temperatures. Cross-section SEM micrographs of b) AgMeF_C_20_20_7d, c) AgMeF_C_40_20_7d, d) AgMeF_C_60_20_7d, e) content of AgNPs (wt.%) of all samples fabricated after 7 days, and f) The values of Lightness ($L^*$) of neat melamine foam (MeF), and samples fabricated using water as solvent at different temperatures.

at 40 °C, and towards dark grey when treated at 60 °C. The inspection of the SEM micrographs of AgMeF foams displayed in Figure 5b–d, showed the bright clusters constituting the silver nanoparticles, as well as the preservation of the cellular structure after applying temperature. Interestingly, Figure 5e showed that samples processed at moderate temperature conditions exhibited a content of AgNPs (wt.%) superior to other foams fabricated in the presence of the toxic solvent THF. In fact, the functionalization degree of AgMeF_C_60_20_7d sample (8.1%) almost duplicated the values obtained for AgMeF_C_20_5_7d (4.2%) and AgMeF_C_20_10_7d (4.8%), while the content of nanoparticles in AgMeF_C_40_20_7d was equivalent to the foams fabricated with THF (4.7%). This improvement of the functionalization yield was expected because temperatures increase the kinetic of the chemical reaction.[53]

The color characterization, represented with the parameters CIE L* (lightness), a* (redness), and b* (yellowness) of each sample, is displayed in Table S3, Supporting Information. These results showed that the sample became darker (lower L*) and lost the coloring red (a*) and yellow (b*). The negative trend of lightness (L*) with respect to the fabrication temperature is represented in Figure 5f. According to the bibliography,[52,55] the optical properties of noble metals nanoparticles are dominated by surface plasmon resonance effect. Generally, the dark-brown tone is a consequence of the formation of agglomeration or a range of particles of a larger size.[17,52] It has been demonstrated that the rise in the reaction temperature causes the modification of the kinetic mechanism of the reaction along with the aggregation of nanoparticles.[53] For example, the synthesis of AgNPs through the reduction of silver nitrate with banana peel extract conducted at different temperatures showed that higher temperatures (80 °C and 100 °C) led to higher particle size or aggregates, and hence, to dark brown colors, while milder temperatures (such as 40 °C and 60 °C) gave place to light brown color.[54] To gain more insight into this, the microstructure of the melamine foams was evaluated under STEM microscopy in the following section.

### 2.6. Effect of Temperature on the Morphology and Distribution of Silver Nanoparticles

The STEM-HAADF micrographs and particle size histograms (inset) of samples fabricated with water at different temperatures (20, 40, and 60 °C) are reported in **Figure 6**a–c. In all samples, silver (white spots) appeared dispersed over all foam surface. The particle average size exhibited a slight upshifting with rising temperature from ≈ 4.8 nm to ≈ 6.5 nm, which is not expected to be responsible for the noticeable color change. The accumulative mass histograms reported in Figure S7, Supporting Information, revealed that the percentage of AgNP bigger than 10 nm was almost doubled when the synthesis temperature reached 60 °C, from ≈ 35% (AgMeF_C_20_20_7d) to ≈ 70% (AgMeF_C_60_20_7d). The study developed by Zhou et al.,[2] reported that the particle size can modify the activity of the silver nanoparticles, for example, ultrafine silver nanoparticles (≈ 9.6 nm) exhibited excellent antibacterial properties, while bigger nanoparticles (≈ 25.3 nm) provided excellent SERS activity.

 

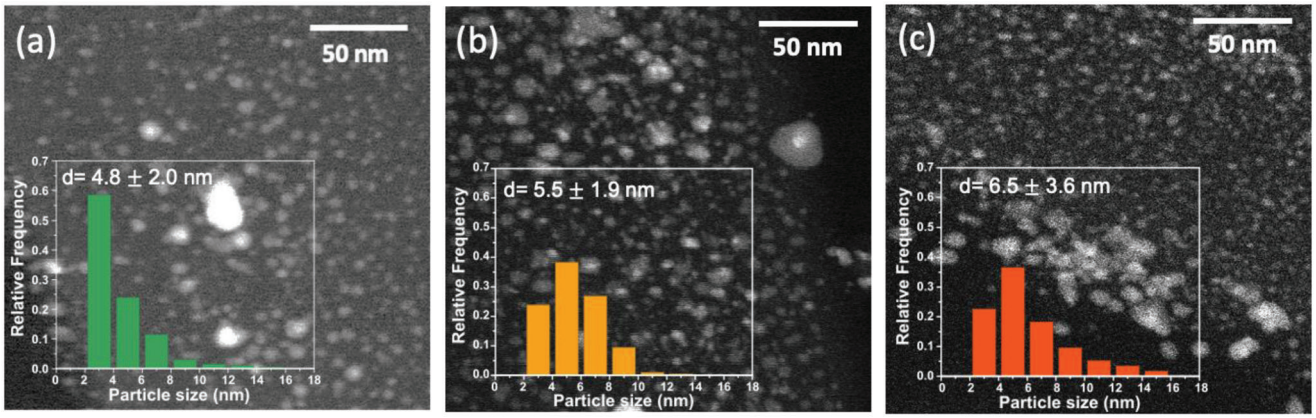


**Figure 6.** HAADF-STEM micrographs and particle size histograms (inset) of a) AgMeF_C_20_20_7d, b) AgMeF_C_40_20_7d, c) AgMeF_C_60_20_7d.

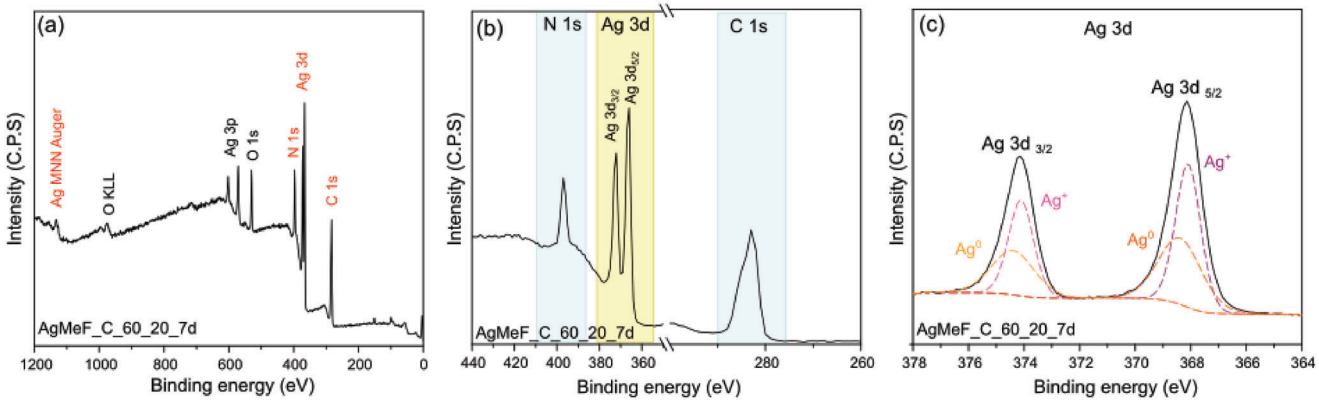


**Figure 7.** a) Wide-scan XPS spectra, b) N 1s, Ag 3d, and C 1s region of XPS spectra, and c) high-resolution XPS spectra of Ag 3d for the representative sample AgMeF_C_60_20_7d.

When compared to the total quantity of AgNPs in melamine foams (agglomerates excluded), the amount of nanoparticles smaller than 10 nm was ≈11.5 mg $g^{-1}$ in AgMeF_C_20_20_7d, 15.6 mg $g^{-1}$ in AgMeF_C_40_20_7d, and 8.5 mg $g^{-1}$ in AgMeF_C_60_20_7d. The noticeable difference with respect to the samples treated with THF (AgMeF_C_20_5_7d and AgMeF_C_20_10_7d), with 42.0 mg $g^{-1}$ and 43.8 mg $g^{-1}$ amount of nanoparticles, was a result of the lower particle size (all below the 10 nm) and the minor amount of aggregates, which were below the 10% of the total silver contained in the foams for both samples. Despite that, the effect of the aggregates on the final performance of the material could be negligible. According to the article Pinto et al.,[24] melamine foams containing a total amount of ≈ 18.0 mg $g^{-1}$ of silver (majority ultrafine without considering the presence of aggregates) showed excellent antibacterial properties, which performance did not improve by increasing the concentration.

As shown in Table S2 of Supporting information, the average size of silver aggregates of these samples increased with increasing the temperature up to reaching a maximum of 1 µm for AgMeF_C_60_20_7d, almost 5 times above the samples processed at room conditions temperature (20 °C). The silver aggregates represented 45.4% and 65.1% of the overall volume of silver nanoparticles present in the foams. Evaluating all these factors (i.e., the quantity of silver, particle size, surface density, and content of aggregates), 40 °C was established as the optimum temperature to obtain melamine foams with ultrafine and well-dispersed silver nanoparticles following a green approach.

Nevertheless, these results evidenced that the presence of aggregates was not enough to explain the relevant differences in color observed in samples. Therefore, the chemical features of the silver nanoparticles will be analyzed hereinafter to better understand the cause of these differences.

### 2.7. Effect of Temperature on the Chemical Features of Melamine Foams

**Figure** 7a exhibits the wide XPS spectra of the AgMeF_C_60_20_7d, which was selected as a representative example. The rest of the samples showed the same XPS spectra with irrelevant differences. The XPS spectra exhibits the peaks of N 1s, C 1s, and O 1s, which are consistent with the elemental composition of melamine foam.[24] The detection of the Ag 3d, Ag 3d, and Ag NMM Auger ($M_5N_{45}N_{45}$) peaks confirmed the presence of AgNPs anchored to the matrix.[24,56] A thoughtful inspection of the XPS peaks marked in red in Figure 7a will be performed to obtain a complete chemical study of the AgMeF

 

**Table 1.** The relative percentage of $Ag^0$ and $Ag^+$ in samples on the basis of peak-fitting of Ag 3d signals.

| Sample | Percentage $Ag^0$ (%) | Percentage $Ag^+$ (%) |
|---|---|---|
| AgMeF_C_20_5_7d | 78.91 | 21.09 |
| AgMeF_C_20_10_7d | 56.64 | 43.36 |
| AgMeF_C_20_20_7d | 67.13 | 32.87 |
| AgMeF_C_40_20_7d | 71.58 | 28.43 |
| AgMeF_C_40_60_7d | 55.6 | 44 |

foams. XPS spectra of AgMeF_C_60_20_7d in the range of 260–440 eV is exhibited in Figure 7b. As said above, the peaks of nitrogen and carbon (N 1s, C 1s) marked in blue were assigned to the backbone of melamine foams. In yellow is highlighted the two characteristic peaks corresponding to the 3d core level of Ag, Ag $3d_{3/2}$ and Ag $3d_{5/2}$, at binding energy 374 eV and 368 eV, respectively.[16,57]

The XPS peaks of Ag 3d were inspected to evaluate the oxidation state of silver. The deconvolution peaks of the Ag $3d_{3/2}$ and Ag $3d_{5/2}$ represented in Figure 7c, suggest the existence of silver in two different oxidation states, $Ag^0$ and $Ag^+$. The displacement of the Auger peaks of Ag, (Auger $M_5N_{45}N_{45}$), confirmed that $Ag^0$ was the main oxidation state of the silver in the studied samples, see Figure S8 of Supporting information.

The ratio between these two species is represented in **Table 1**. The relative amount of $Ag^0$ with respect to $Ag^+$ varied from 55% to 79%, increasing with the THF solvent ratio. The reduction of reaction efficiency with water, in terms of producing $Ag^0$, was supported by the results reported in Pinto et al.,[24] which MeF, fabricated with a solvent mixture of $H_2O$/THF (1:19 v:v), present only a 13 wt.% of relative amount of $Ag^+$. Interestingly, previous results show that silver nanoparticles preserve their antibactericide response in both oxidation states (0, +1), being capable of releasing $Ag^+$ proportionally to the concentration of nanoparticles.[12,50] In fact, some studies revealed that the $Ag^+$ nanoparticles, in the form of $Ag_2O$, could exhibit faster and more efficient bactericide activities with respect to zerovalent Ag, which means that the silver oxidation does not represent a drawback for the potential application of the foams.[50]

Regarding the notorious color differences between the samples, the presence of silver oxide ($Ag_2O$), which exhibits a characteristic black or dark brown color, in combination with the presence of silver agglomerates, can justify the different appearance of the samples exhibited in **Figure 8**. For example, the high concentration of $Ag_2O$ of AgMeF_C_20_10_7d (above 40%) could explain the noticeable darkening with respect to the AgMeF_C_20_5_7d sample, with similar particle size distribution (see Figure 4a) and minor content of agglomerates (<10%). On the other side, the darker color of the samples processed with water at higher temperatures can be mainly associated with

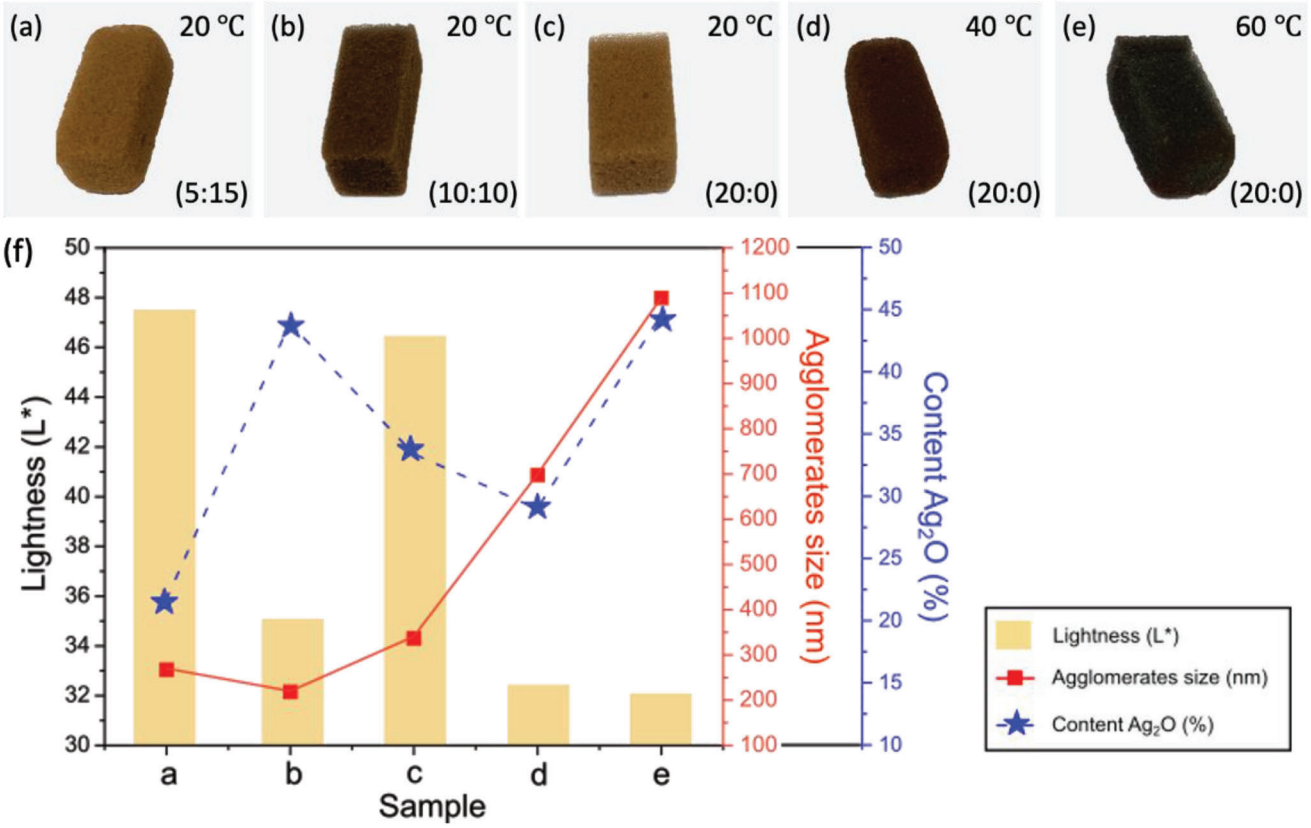


**Figure 8.** Photographs of samples treated under stirring for seven days with different $H_2O$/THF ratios and temperature conditions: a) 5:15 and 20 °C, b) 10:10 and 20 °C, c) 20:0 and 20 °C, d) 20:0 and 40 °CC, and e) 20:0 and 60 °C, f) Representation of the Lighness ($L^*$) of samples (yellow) against the agglomerates size (in red) and the content of $Ag_2O$ (in blue).

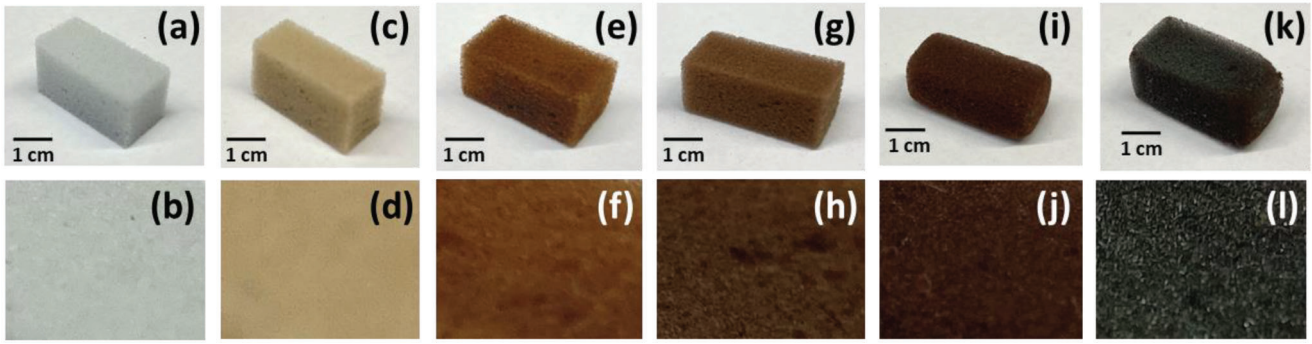


**Figure 9.** Photographs of representative samples of melamine foams a,b) neat melamine (MeF), melamine reacting with $AgNO_3$ in static c,d) in $H_2O$: THF solvent volume ratio of 5:15 for three days, and e,f) in $H_2O$: THF solvent volume ratio (10:10) for five days. Samples were fabricated in water solution for 7 days in stirring at different temperatures g,h) 20 °C, i,j) 40 °C, and k,l) 60 °C.

the presence of agglomerates, presented in 45.4% and 65.1% for AgMeF_C_40_20_7d and AgMeF_C_60_20_7d, respectively. Whereas for the sample AgMeF_C_60_20_7d, its appearance was also influenced by the noticeable presence of silver oxide, which reached more than 40%.

Nevertheless, it should be highlighted that sample AgMeF_C_40_20_7d, previously appointed as the optimum sample achieved by a green method, in terms of ultrafine Ag NPs functionalization and contents of $Ag^+$, similar to those of foams prepared with THF.

## 3. Conclusions

An alternative green route for the functionalization of melamine foams with silver nanoparticles has been successfully implemented in this work. The detailed study of several fabrication conditions indicated that the reaction time, stirring, and higher THF ratio with respect to water, displayed a positive effect on the content of silver in the foams. However, these results also evidenced that samples processed only in water could reach similar or even higher functionalization degrees when an increment of temperature is applied. The reaction yield showed to be greatly enhanced with the rising temperature, obtaining 4.7% and 8.1% of Ag NPs in foams processed at 40 °C and 60 °C, while the maximum performance of Ag NPs obtained using THF was 4.8%. Despite the temperature prompted the formation of aggregates, 45.4% (AgMeF_C_40_20_7d) and 65.0% (AgMeF_C_60_20_7d) with respect to the total silver in foams, they exhibited well-dispersed and small nanoparticles, a great percentage in the range of ultrafine nanoparticles (<10 nm).

Results manifested that the variations in the relative content of $Ag^+$ (mainly $Ag_2O$), as well as the increment of the aggregates size (although they represented insignificant volume fractions), were responsible for a darker color on samples like AgMeF_C_20_10_7d, and AgMeF_C_60_20_7d.

Among all fabrication conditions, melamine foams stirred for 7 days in the precursor solution ($AgNO_3$ and water) at 40 °C was selected as the sample with the best characteristics. This sample, produced by a green approach, presents a proper dispersion of nanoparticles and contained the greater amount of AgNPs among the samples produced without using hazardous solvents (≈15.2 mg $g^{-1}$ foam) with a particle size below 10 nm, a major content of $Ag^0$. After this treatment, the porous melamine structure kept unspoiled, and its outstanding functionalization yield overcame most of the materials found in the literature.

## 4. Experimental Section

*Materials*: Commercial Melamine foams (MeF) were kindly provided by Flexicel Industrial S.L. (Spain). These foams presented a very high porosity (0.994), open pores, and a mean pore size below 500 µm. Tetrahydrofuran (THF) and silver nitrate ($AgNO_3$) were purchased from Scharlab S.L. (Spain). Deionized water was obtained from a RiOs-DI 3 Water Purification device. Common commercial ethanol (96%) for medical applications was employed to rinse the samples.

*Preparation of Functionalized AgNPs-MeF*: Commercial samples of pristine MeF (2 × 1 × 1 $cm^3$) were rinsed in ethanol and THF to ensure the elimination of the remaining impurities that could be formed during the industrial fabrication process.[24] Then, they were immersed in 20 mL of 1.7 mg $mL^{-1}$ $AgNO_3$ solutions with different solvent volume ratios, $H_2O$:THF (5:15, 10:10, 20:0 v:v) for a certain time (ranging from 1 to 7 days). The redox reaction undergone in the Ag precursor solution was studied at room temperature (≈ 20 °C) under three different kinetic conditions: static, shaking in a Heidolph Multi Reax Vortex mixer at 300 rpm, and stirring on a hot plate at 300 rpm. Then, samples were removed from the precursor solution and exposed to 5 washing cycles with distilled water to remove the THF, or nonbonding $AgNO_3$, and AgNPs that remained after the synthesis process.[24] Finally, samples were left to dry under the hood overnight before the characterization. Photographs of some representative samples are displayed in **Figure 9**. As observed, all samples exhibited different colors associated with the formation of silver nanoparticles anchored to the foam with certain chemical and structural features, like oxidation state or different dispersion and particle size.[24,41] In addition to this, the effect of the temperature on the MeF functionalization was studied for the samples with a solvent volume ratio $H_2O$:THF (20:0 v:v, i.e., pure distilled water). In this case, pristine MeF was put to stir at 300 rpm in the precursor solution on a hot plate heated at 40 °C and 60 °C for 7 days. The obtained samples were compared with those produced following the same route (i.e., stirring) at room temperature and using the same solvent ratio.

The sample labeling criteria and fabrication details are reported in **Table 2**. Other MeF samples were also soaked in the different solvent ratios $H_2O$: THF (0:20, 5:15, 10:10, and 20:0 v:v) without silver salts to test the effect of the solvent in the matrix. These foams were labeled as MeF_A_20_7_0, MeF_A_20_7_5, MeF_A_20_7_10, and MeF_A_20_7_20, for each solvent ratio respectively. The influence of temperature was also evaluated in neat melamine samples labeled as MeF_C_40_7_20 and MeF_C_60_7_20.

**Table 2.** The labeling and fabrication parameters of all samples. Acronyms were defined as follows AgMeF_procedure_temperature_water volume ratio_time.

| Procedure | Temperature (°C) | Time (days) | Solution $H_2O$: THF (v: v) | | |
|---|---|---|---|---|---|
| | | | 5:15 | 10:10 | 20:0 |
| Static (A) | 20 | 1 | AgMeF_A_20_5_1d | AgMeF_A_20_10_1d | AgMeF_A_20_20_1d |
| | | 3 | AgMeF_A_20_5_3d | AgMeF_A_20_10_3d | AgMeF_A_20_20_3d |
| | | 5 | AgMeF_A_20_5_5d | AgMeF_A_20_10_5d | AgMeF_A_20_20_5d |
| | | 7 | AgMeF_A_20_5_7d | AgMeF_A_20_10_7d | AgMeF_A_20_20_7d |
| Shaking (B) | 20 | 1 | AgMeF_B_20_5_1d | AgMeF_B_20_10_1d | AgMeF_B_20_20_1d |
| | | 3 | AgMeF_B_20_5_3d | AgMeF_B_20_10_3d | AgMeF_B_20_20_3d |
| | | 5 | AgMeF_B_20_5_5d | AgMeF_B_20_10_5d | AgMeF_B_20_20_5d |
| | | 7 | AgMeF_B_20_5_7d | AgMeF_B_20_10_7d | AgMeF_B_20_20_7d |
| Stirring I | 20 | 1 | AgMeF_C_20_5_1d | AgMeF_C_20_10_1d | AgMeF_C_20_20_1d |
| | | 3 | AgMeF_C_20_5_3d | AgMeF_C_20_10_3d | AgMeF_C_20_20_3d |
| | | 5 | AgMeF_C_20_5_5d | AgMeF_C_20_10_5d | AgMeF_C_20_20_5d |
| | | 7 | AgMeF_C_20_5_7d | AgMeF_C_20_10_7d | AgMeF_C_20_20_7d |
| | 40 | 7 | – | – | AgMeF_C_40_20_7d |
| | 60 | 7 | – | – | AgMeF_C_60_20_7d |

*Scanning Electron Microscopy (SEM)*: The study of the cross-section morphology of pristine MeF was performed with a scanning electron microscopy (SEM) HITACHI FlexSEM 1000. Neat samples of melamine were coated with gold (10 nm) and the measurement was performed using an accelerating voltage of 10 kV and a secondary electron detector (SED). The melamine foams containing silver nanoparticles (AgMeF) were not coated and the micrographs were taken using an accelerating voltage of 15 kV and with a backscattered electrons detector to highlight the presence of silver nanoparticles.

*Attenuated Total Reflection Fourier Transform Infrared (ATR-FTIR)*: The infrared spectra were collected using a Bruker Tensor 27 spectrometer working in Attenuated Total Reflectance (ATR) method with an MKII Golden-Gate accessory. Each FTIR spectrum was obtained at room temperature after 32 scans, with a resolution of 4 $cm^{-1}$ in the range 4000–600 $cm^{-1}$. All IR spectra were normalized by the peak 1480 $cm^{-1}$, corresponding to the bending vibration mode of the methylene group.[44]

*Thermogravimetric Analysis (TGA)*: Thermal gravimetric analysis (TGA) was performed using a SDTA851, Metter Toledo instrument. The temperature was set in a range from 50 °C to 800 °C with a heating rate of 20 °C $min^{-1}$ under a nitrogen atmosphere with a constant flow rate of 60 mL $min^{-1}$, followed by an isotherm at 800 °C for 15 min under air atmosphere with a constant flow rate of 200 mL $min^{-1}$. The remaining residue after the calcination of functionalized foams (AgMeFs) was utilized to quantify the silver nanoparticles in the sample. The untreated melamine foam (MeF) was employed as a reference for the calculating residue obtained for each AgMeF sample.[41]

*Scanning Transmission Electron Microscopy (STEM)*: For the preparation of STEM specimens of the Ag Foams, different fragments of each sample were cut with a razor blade and dehydrated with ethanol. Afterward, samples were embedded in fresh EMBed 812 epoxy resin and cut at room temperature with a diamond knife on a Leica EM UC7 ultramicrotome device. Ultrathin sections of 70-nm thick cross-section membranes were mounted on carbon 200 mesh copper grids. STEM observations were carried out with a F30-FEI microscope with a X electron source at STEM mode. Microscopy images were recorded using a high-angle annular dark field detector (STEM-HAADF) in a FEI XFEG TITAN electron microscope operated with a working voltage of 300 kV. The elemental analysis of the sample surface was obtained with Energy-dispersive X-ray spectroscopy (EDS) using a EDAX detector. High-resolution TEM (HRTEM) images were used for a deeper inspection of the morphology of the silver nanoparticles. In this case, the image acquisition was carried out using a coupled CCD camera (Gatan).

*Analysis of Silver Nanoparticles and Aggregates*: The surface number density of Ag nanoparticles ($N_{NPs}$) or Ag agglomerates ($N_{Agg}$) was calculated using Equation (1), where n is the number of Ag nanoparticles or aggregates present in a surface of the foams with area A. For performing this calculation, the surface density of nanoparticles ($N_{NPs}$) was calculated from HRTEM images, while the surface density of aggregates ($N_{Agg}$) was estimated from SEM images at high magnifications, in both cases using the image processing software ImageJ. It should be noticed that in the case of Ag aggregates the effective foam surface for these calculations was obtained by considering the relative density of the foams (e.g., volume fraction of the polymer matrix). The average volume of silver (AgNPs or aggregates) was calculated considering a spherical shape for both silver nanoparticles and aggregates, according to HRTEM images. Same to the analysis of surface density, the average diameter of silver nanoparticles ($r_{NPs}$) was calculated from HRTEM images, while the diameter of aggregates ($r_{Agg}$) was estimated from SEM images at high magnifications using the image processing software ImageJ. Then, the volume fraction of aggregates ($V_{Agg}$), with respect to the total volume of silver (AgNPs and aggregates), was estimated from Equation (2).

$$N_{NPs/Agg}\ \left(\text{number of Ag nanoparticles or aggregates/mm}^2\right) = n_{NPs/Agg}\ /A \quad (1)$$

$$V_{Agg}\ (\%) = \frac{N_{Agg}\ x\ \frac{4}{3}\pi {r_{Agg}}^3}{N_{Agg}\ x\ \frac{4}{3}\pi {r_{Agg}}^3 + N_{NPs}\ x\ \frac{4}{3}\pi {r_{NPs}}^3}\ \text{x}\ 100 \quad (2)$$

*Colorimetry Study*: Color measurements were performed using a commercial color reader Colourpin SE (NCS Color AB, USA), using a standard illumination D65, 10° standard observer were used. This color reader provides the color coordinates of the samples on the standard color space CIE $L^*a^*b^*$, where there are three axes orthogonal to each other: measurable lightness $L^*$ (values range from 0 (black) to 100 (white); and two chromatic axes $a^*$ (values from green (negative) to red (positive), and $b^*$ (values from blue (negative) to yellow (positive).

*X-Ray Photoelectron Spectroscopy (XPS) Analysis*: X-ray photoelectron spectra of samples were taken using a XPS Spectrometer Kratos AXIS Supra. Monochromatic Al-$K_\alpha$ source with photon energy 1486.6 eV was used, operating with an emission current of 8 mA, 15 kV, and at $10^{-9}$ Torr. For the quantitative analysis, the energy calibration was performed by

 

setting the C–C/C–H component of the C 1s spectrum to a fixed binding energy value of 284.5 eV.

## Supporting Information

Supporting Information is available from the Wiley Online Library or from the author.

## Acknowledgements

Financial assistance from Ministerio de Ciencia e Innovación (Spain) (PID2021-127108OB-I00), MCIN/AEI /10.13039/501100011033 and the EU NextGenerationEU/ PRTR program PLEC2021-007705), Ministerio de Ciencia, Innovación y Universidades (MCIU) (Spain), FEDER (EU) (RTI2018 – 098749-B-I00 and RTI2018 – 097367-A-I00), Regional Government of Castilla y León and the EU-FEDER program (CLU-2019-04 and VA202P20), and Ministerio de Ciencia e Innovación, EU NextGenerationEU/ PRTR program, Regional Government of Castilla y León, and EU-FEDER program "Plan Tractor En Materiales Avanzados Enfocado A Los Sectores Industriales Claves En Castilla Y León: Agroalimentario, Transporte, Energía Y Construcción (MA2TEC)", JCyL and European Regional Development Fund for funding the Projects CLU-2019-04 were gratefully acknowledged. This research was funded by the European Union–NextGenerationEU and the University of Valladolid, within the Margarita Salas program, grant number CONVREC-2022-63. The authors would like to acknowledge the use of Servicio General de Apoyo a la Investigación-SAI, Universidad de Zaragoza.

## Conflict of Interest

The authors declare no conflict of interest.

## Data Availability Statement

Research data are not shared.

## Keywords

green synthesis, polymer foams, reaction conditions, silver reduction

Received: May 18, 2023
Revised: June 28, 2023
Published online: September 28, 2023

[1] J. Dobias, R. Bernier-Latmani, *Environ. Sci. Technol.* **2013**, *47*, 4140.
[2] Y. Zhou, J. Huang, W. Shi, Y. Li, Y. Wu, Q. Liu, J. Zhu, N. Zhao, L. Zhang, J. Yang, X. Cheng, *Appl. Surf. Sci.* **2018**, *457*, 1000.
[3] B. Calderón-Jiménez, M. E. Johnson, A. R. Montoro Bustos, K. E. Murphy, M. R. Winchester, J. R. Vega Baudrit, *Front. Chem.* **2017**, *5*, 6.
[4] L. Wang, S. Chen, J. Zhou, J. Yang, X. Chen, Y. Ji, X. Liu, L. Zha, *Macromol. Mater. Eng.* **2017**, *302*, 1700181.
[5] K. B. R. Teodoro, F. L. Migliorini, W. A. Christinelli, D. S. Correa, *Carbohydr. Polym.* **2019**, *212*, 235.
[6] S. Davidovic, V. Lazic, I. Vukoje, J. Papan, S. P. Anhrenkiel, S. Dimitrijevic, J. M. Nedeljkovic, *Colloids Surf., B* **2017**, *160*, 184.
[7] D. C. M. Ferreira, G. F. Giordano, C. C. D. S. P. Soares, J. F. A. De Oliveira, R. K. Mendes, M. H. Piazzetta, A. L. Gobbi, M. B. Cardoso, *Talanta* **2015**, *141*, 188.
[8] E. Fortunati, M. Peltzer, I. Armentano, A. Jiménez, J. M. Kenny, *J. Food Eng.* **2013**, *118*, 117.
[9] S. Sun, S. Tang, X. Chang, N. Wang, D. Wang, T. Liu, Y. Lei, Y. Zhu, *Appl. Surf. Sci.* **2019**, *473*, 1049.
[10] C.-H. Deng, J.-L. Gong, P. Zhang, G.-M. Zeng, B. Song, H.-Y. Liu, *J. Colloid Interface Sci.* **2017**, *488*, 26.
[11] A. G. Morena, I. Stefanov, K. Ivanova, S. Pérez-Rafael, M. Sánchez-Soto, T. Tzanov, *Ind. Eng. Chem. Res.* **2020**, *59*, 4504.
[12] J. Pinto, S. Barroso-Solares, D. Magrì, F. Palazon, S. Lauciello, A. Athanassiou, D. Fragouli, *Polymers* **2020**, *12*, 934.
[13] B. Le Ouay, F. Stellacci, *Nano Today* **2015**, *10*, 339.
[14] A. K. Karumuri, D. P. Oswal, H. A. Hostetler, S. M. Mukhopadhyay, *Mater. Lett.* **2013**, *109*, 83.
[15] F. Brako, C. Luo, D. Q. M. Craig, M. Edirisinghe, *Macromol. Mater. Eng.* **2018**, *303*, 1700586.
[16] H. Shen, A. J. Gulbrandson, S. Park, M. Li, D. Shuai, P. C. Trulove, D. P. Durkin, *Macromol. Mater. Eng.* **2022**, *307*, 2100872.
[17] M. Villalpando, G. Rosas, *Microsc. Microanal.* **2019**, *25*, 1976.
[18] C. Wang, K. W. Wong, Q. Wang, Y. Zhou, C. Tang, M. Fan, J. Mei, W.-M. Lau, *Talanta* **2019**, *191*, 241.
[19] A. Serra, E. Filippo, M. Re, M. Palmisano, M. Vittori-Antisari, A. Buccolieri, D. Manno, *Nanotechnology* **2009**, *20*, 165501.
[20] K. Nesovic, V. Miskovic-Stankovic, *Polym. Eng. Sci.* **2020**, *60*, 1393.
[21] M. Azizi-Lalabadi, F. Garavand, S. M. Jafari, *Adv. Colloid Interface Sci.* **2021**, *293*, 102440.
[22] S. Barroso-Solares, B. Merillas, P. Cimavilla-Román, M. A. Rodriguez-Perez, J. Pinto, *J. Clean Prod.* **2020**, *254*, 120038.
[23] J.-T. Zhang, G. Wei, T. F. Keller, H. Gallagher, C. Stötzel, F. A. Müller, M. Gottschaldt, U. S. Schubert, K. D. Jandt, *Macromol. Mater. Eng.* **2010**, *295*, 1049.
[24] J. Pinto, D. Magrì, P. Valentini, F. Palazon, J. A. Heredia-Guerrero, S. Lauciello, S. Barroso-Solares, L. Ceseracciu, P. P. Pompa, A. Athanassiou, D. Fragouli, *ACS Appl. Mater. Interfaces* **2018**, *10*, 16095.
[25] T. Huang, S. Cao, D. Luo, N. Zhang, Y.-Z. Lei, Y. Wang, *Chemosphere* **2022**, *287*, 132054.
[26] Q. Ren, T. Dai, X. Jin, D. Wu, C. Wang, J. Li, S. Zhu, *Macromol. Mater. Eng.* **2018**, *303*, 1800436.
[27] C. Yan, Y.-J. Luo, W.-G. Zhang, Z.-F. Zhu, P.-Y. Li, N. Li, Y.-F. Chen, T. Jin, *J. Appl. Polym. Sci.* **2021**, *139*, 51992.
[28] Q. Li, J.-J. Liu, X. Sun, L. Xu, *ACS Sustainable Chem. Eng.* **2019**, *7*, 867.
[29] M. Alizadeh-Bavieh, V. Nobakht, T. Sedaghat, L. Carlucci, P. Mercandelli, M. Taghavi, *J. Solid State Chem.* **2021**, *294*, 121855.
[30] M. Kavsek, N. Figar, I. Mihelic, M. Krajnc, *J. Cell. Plast.* **2021**, *58*, 175.
[31] R. Guo, X. Han, P. Yuan, X. He, Q. Li, J. Sun, L. Dang, Z. Liu, Y. Zhang, Z. Lei, *Nano Res.* **2021**, *15*, 3254.
[32] Z. Li, X. Xu, H. Quan, J. Zhang, Q. Zhang, Y. Fu, Y. Ying, Y. Li, *Chem. Eng. J.* **2021**, *410*, 128268.
[33] L. Zhang, L. Feng, X. Gu, C. Zhang, *J. Appl. Polym. Sci.* **2021**, *138*, 50038.
[34] X. Lv, D. Tian, Y. Peng, J. Li, G. Jiang, *Appl. Surf. Sci.* **2019**, *466*, 937.
[35] J. J. Martin, J. M. Cardamone, P. L. Irwin, E. M. Brown, *Colloids Surf., B* **2011**, *88*, 354.
[36] S. Farhan, R. Wang, K. Li, *J. Mater. Sci.* **2016**, *51*, 7991.
[37] H. Ren, H. Li, H. Wang, H. Huang, Z. Lu, *Microorganisms* **2020**, *8*, 1190.
[38] A. O. Gamer, R. Jaeckh, E. Leibold, W. Kaufmann, C. Gembardt, R. Bahnemann, B. van Ravenzwaay, *Toxicol. Sci.* **2002**, *70*, 140.
[39] A. P. M. Loureiro, I. P. De Arruda Campos, O. F. Gomes, E. P. M. Possari, P. Di Mascio, M. H. G. Medeiros, *Chem. Res. Toxicol.* **2006**, *18*, 290.
[40] L. A. Malley, G. R. Christoph, J. C. Stadler, J. F. Hansen, J. A. Biesemeier, S. L. Jasti, *Drug Chem Toxicol* **2001**, *24*, 201.
[41] S. Barroso-Solares, P. Cimavilla-Roman, M. A. Rodriguez-Perez, J. Pinto, *Polymers* **2020**, *12*, 996.

 

[42] X. Yuan, K. Luo, K. Zhang, J. He, Y. Zhao, D. Yu, *J. Phys. Chem. A* **2016**, *120*, 7427.
[43] N. E. Mircescu, M. Oltean, V. Chis, N. Leopold, *Vib. Spectrosc.* **2012**, *62*, 165.
[44] A. Stolz, S. Le Floch, L. Reinert, S. M. M. Ramos, J. Tuaillon-Combes, Y. Soneda, P. Chaudet, D. Baillis, N. Blanchard, L. Duclaux, A. San-Miguel, *Carbon* **2016**, *107*, 198.
[45] J. Li, W. Zhang, S. Xu, C. Hu, *Front. Chem.* **2020**, *8*, 70.
[46] Q. Yan, Z. Cai, *Molecules* **2020**, *25*, 2167.
[47] M. Taghizadeh, M. H. Abbandanak, *Int. J. Hydrogen Energy* **2022**, *47*, 16362.
[48] M. Tao, X. Meng, Y. Lv, Z. Bian, Z. Xin, *Fuel* **2016**, *165*, 289.
[49] S.-C. Lin, C.-C. M. Ma, S.-T. Hsiao, Y.-S. Wang, C.-Y. Yang, W.-H. Liao, S.-M. Li, J.-A. Wang, T.-Y. Cheng, C.-W. Lin, R.-B. Yang, *Appl. Surf. Sci.* **2016**, *385*, 436.
[50] D.-N. Phan, N. Dorjjugder, Y. Saito, G. Taguchi, H. Lee, J. S. Lee, I.-S. Kim, *Mater. Today Commun.* **2019**, *21*, 100622.
[51] D. Archana, B. K. Singh, J. Dutta, P. K. Dutta, *Int. J. Biol. Macromol.* **2015**, *73*, 49.
[52] F. M. Kelly, J. H. Johnston, *ACS Appl. Mater. Interfaces* **2011**, *3*, 1083.
[53] S. Piñero, S. Camero, S. Blanco, *J. Phys.: Conf. Ser.* **2017**, *786*, 012020.
[54] A. Bankar, B. Joshi, A. R. Kumar, S. Zinjarde, *Colloids Surf., A* **2010**, *368*, 58.
[55] A. Paghi, M. Corsi, S. Corso, S. Mariani, G. Barillaro, *Nanoscale Horiz.* **2022**, *7*, 425.
[56] A. Machocki, T. Ioannides, B. Stasinska, W. Gac, G. Avgouropoulos, D. Delimaris, W. Grzegorczyk, S. Pasieczna, *J. Catal.* **2004**, *227*, 282.
[57] A. Fahmy, K. S. El-Nasser, I. O. Ali, T. M. Salama, K. Altmann, J. Friedrich, *J. Adhes. Sci. Technol.* **2017**, *31*, 2641.

 